OBSERVATIONS OF RECONNECTING FLARE LOOPS WITH THE ATMOSPHERIC IMAGING ASSEMBLY (AIA)

Harry P. Warren, Casey M. O'Brien[1], Neil R. Sheeley, Jr.
Space Science Division, Naval Research Laboratory, Washington, DC 20375
Draft version September 13, 2011

ABSTRACT

Perhaps the most compelling evidence for the role of magnetic reconnection in solar flares comes from the supra-arcade downflows that have been observed above many post-flare loop arcades. These downflows are thought to be related to highly non-potential field lines that have reconnected and are propagating away from the current sheet. We present new observations of supra-arcade downflows taken with the Atmospheric Imagining Assembly (AIA) on the *Solar Dynamics Observatory* (*SDO*). The morphology and dynamics of the downflows observed with AIA provide new evidence for the role of magnetic reconnection in solar flares. With these new observations we are able to measure downflows originating at much larger heights than in previous studies. We find, however, that the initial velocities measured here ($\sim$144 km s^{-1}) are well below the Alfvén speed expected in the lower corona, and consistent with previous results. We also find no evidence that the downflows brighten with time, as would be expected from chromospheric evaporation. These observations suggest that simple two-dimensional models cannot explain the detailed observations of solar flares.

Subject headings: Sun: corona

1. INTRODUCTION

Magnetic reconnection is a fundamental process in astrophysical plasmas and is believed to be responsible for a wide range of solar phenomena, including solar flares (for a review see Zweibel & Yamada 2009). Unfortunately, magnetic reconnection occurs on spatial scales that are too small to be resolved with current solar instrumentation and cannot be observed directly. There is, however, considerable indirect evidence that magnetic reconnection plays a central role in solar flares. Perhaps the most compelling piece of indirect evidence is the supra-arcade downflows that have been observed above many post-flare loop arcades (e.g., Savage & McKenzie 2011; Savage et al. 2010; Sheeley et al. 2004; Asai et al. 2004; Innes et al. 2003; McKenzie & Hudson 1999). These downflows appear to be related to highly non-potential field lines that have reconnected and are propagating away from the current sheet.

Supra-arcade downflows have been observed with a number of instruments and their properties are summarized in the comprehensive review by Savage & McKenzie (2011). The downlows often appear as dark, collapsing features that look like small "tadpoles" (voids with a trailing dark tail). Some downflows have a loop-like appearance while others appear to evolve from voids into loops. The downflows generally begin at relatively high velocities (100–200 km s^{-1} is typical) and then quickly decelerate to about 4 km s^{-1}. Observations at high spatial resolution give the impression that much of high temperature plasma in a flare is formed from collapsing loops (Sheeley et al. 2004), even when individual features cannot be tracked. Similar features are observed in the outer corona when the streamer belt is viewed face on (e.g., Wang et al. 1999; Sheeley et al. 2001; Sheeley & Wang 2001).

Despite the extensive analysis of previous observations a number of questions remain regarding the downflows and their relationship to magnetic reconnection. The initial velocities measured for the downflows tend to be much smaller than the estimated Alfvén speed in the lower corona

($\sim$1000 km s^{-1}), the velocity expected for reconnection outflows. It is possible that the downflows are formed at large heights and are observed only after they have experienced some deceleration. In most models of solar flares the release of energy in the corona ultimately drives chromospheric evaporation and leads to the formation of hot, dense loops (e.g., Fisher et al. 1985; Mariska et al. 1989). Many of the downflows, however, are observed as dark features and it is not clear that all of the high temperature emission in the flare is formed from descending loops. Finally, why some downflows appear as voids and while others appear as loops is unclear. It is possible that the observed morphology is strongly influenced by the viewing angle.

The launch of the Atmospheric Imaging Assembly (AIA) on the *Solar Dynamics Observatory* (*SDO*) provides a new opportunity to investigate the dynamics of newly reconnected flux tubes in solar flares. AIA has several advantages over previous solar EUV imagers, including a higher cadence (12 s) and more channels that observe at flare temperatures. The higher cadence allows us to create data sets optimized for observing the downflows at large heights. The AIA 94 Å and 131 Å channels observe emission from Fe xviii and Fe xxi, respectively. These lines are formed close to 10 MK, the temperature at which the flare emission measure generally peaks.

Observations from the twin *STEREO* spacecraft (Howard et al. 2008) can also be applied to this problem. During the 2010–2012 time frame the spacecraft are approximately 90° from the Earth-Sun line, which allows flares to be observed simultaneously as limb events by AIA and disk events by the EUVI imagers on *STEREO*.

In this paper we report new observations of supra-arcade downflows taken with AIA and EUVI. With the improved capabilities of AIA we are able to track features at larger heights and in much weaker events than in previous studies. The combined AIA and EUVI observations provide compelling evidence that the downflowing voids and loops are manifestations of the same phenomenon observed along different lines of sight. We find, however, that the initial velocities are consistent with previous measurements and well below the esti-

[1] Massachusetts Institute of Technology, Cambridge, MA 02139 USA.

mated Alfvén speed. The relationship between the brightest emission in the flare and the downflows is also not resolved. We find no evidence that the emission from the downflows rises with time, as would be expected from chromospheric evaporation. Also, for these events the initial high temperature flare loops are observed to form almost "in place" with very little associated downward motion. These difficulties suggest that simple two-dimensional models of magnetic reconnection cannot be applied directly to detailed observations of solar flares.
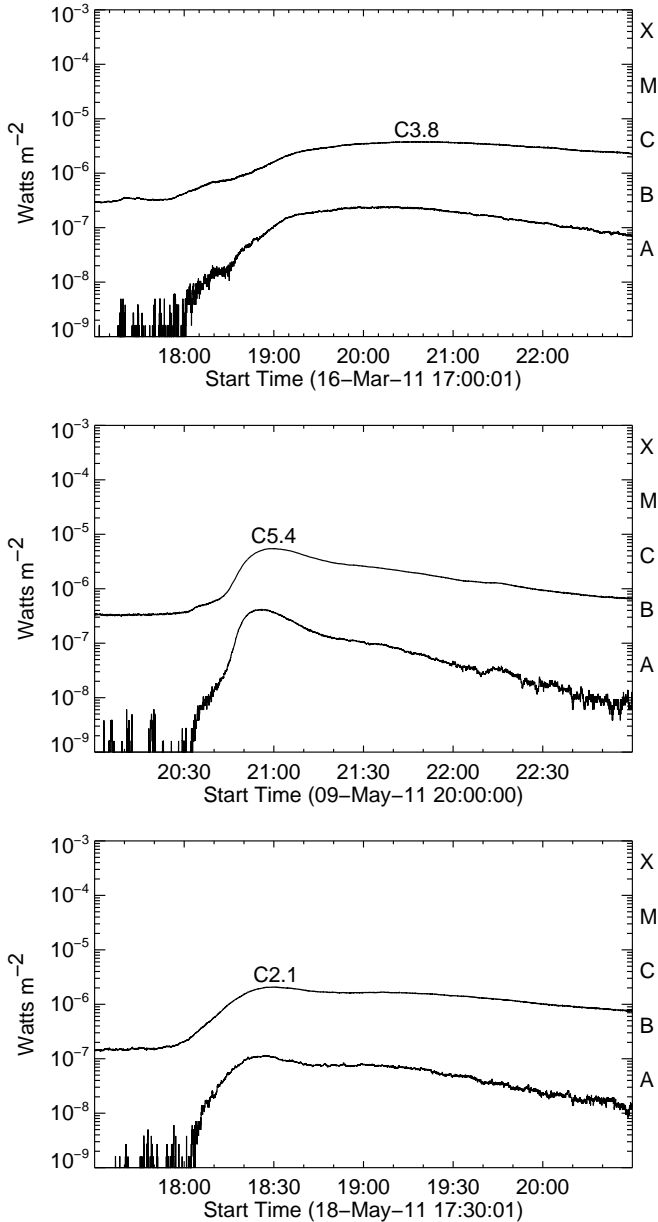
2. OBSERVATIONS

FIG. 1.— Soft X-ray light curves observed with *GOES* 15 for three limb flares. The May 9 and May 18 events are partially occulted.

The AIA instrument on *SDO* is a multilayer imaging telescope. A full description of the instrument is given in Lemen et al. (2011). In brief, the AIA instrument images the full Sun in 10 different channels with $0.6''$ pixels at a typical cadence of 12 s. There are 7 EUV channels for imaging emission from the transition region and corona. The AIA 94 Å, 131 Å, and 193 Å channels observe flare emission from Fe XVIII, Fe XXI, and Fe XXIV, respectively. Each of the channels is also sensitive to emission formed at cooler temperatures. The 193 Å channel includes Fe XII 195 Å, which is an intrinsically bright line and makes Fe XXIV difficult to observe in smaller events. The lower temperature response for the 131 Å channel is primarily from Fe VIII emission lines that are much weaker than Fe XII 195 Å, making the high temperature emission much easier to observe. The lower temperature lines in the 94 Å bandpass are largely unidentified, but they are also relatively weak. For a more complete description of the AIA temperature response see O'Dwyer et al. (2010).

All of the AIA data that we have analyzed are sub-fields of the full disk images obtained from the LMSAL cutout service. The data has been processed using `aia_prep` to remove any energetic particle spikes and co-register the images from the different wavelengths to a common plate scale.

For this work we consider three flares that occurred at the solar limb as viewed from Earth: a C3.8 event that began at about 18:00 UT on 2011 March 16, a C5.4 flare that began at about 20:30 UT on 2011 May 9, and a C2.1 flare that begin at about 18:00 UT on 2011 May 18. The soft X-ray light curves from the *GOES* 15 spacecraft are shown in Figure 1. The *GOES* light curves indicate that these flares are all long duration events that evolve over many hours.

Some representative AIA 131 Å images are shown in Figures 2, 3, and 4. All three events are clearly associated with a coronal mass ejection and have the classic morphology of a two-ribbon flare. Each event shows a diffuse "cloud" of high temperature (~ 10 MK) plasma that rises with time. Over time relatively narrow, lower temperature (~ 1 MK) loops form at the lowest heights and material is observed to drain back down to the surface of the Sun along these loops. The temperatures that we give here are approximate and based on comparisons with previous work (e.g., Warren et al. 1999). High temperature emission is observed only in the 94 and 131 Å channels while only low temperature loops are observed in channels such as 171 Å, which has a significant response only at low temperatures. Very little Fe XXIV emission is observed in the 193 Å channel images for these flares. The *GOES* soft X-ray fluxes for these events are approximately 100 times smaller than was observed in the X-class flares considered previously (e.g., Sheeley et al. 2004; Asai et al. 2004), so this is not surprising.

Movies of the data for each event show evidence for features forming at large heights and descending onto the accumulating post-flare loop arcade. These features are generally difficult to track in the raw intensity images. To eliminate the contribution of the more slowly varying emission it is useful to compute running difference images. With the high cadence of AIA we have considerable flexibility in constructing these images. Through trial and error we have found that averaging sets of 7 images taken 72 s apart produced the best results. Since the downflows move at relatively high velocities, too much averaging or too long an interval between frames blurs the features. Averaging fewer frames or choosing a shorter interval between frames leads to noisier difference images. Example running difference images are displayed in Figures 2, 3, and 4. Movies of the running difference images, which are available in the electronic version of the manuscript, show the
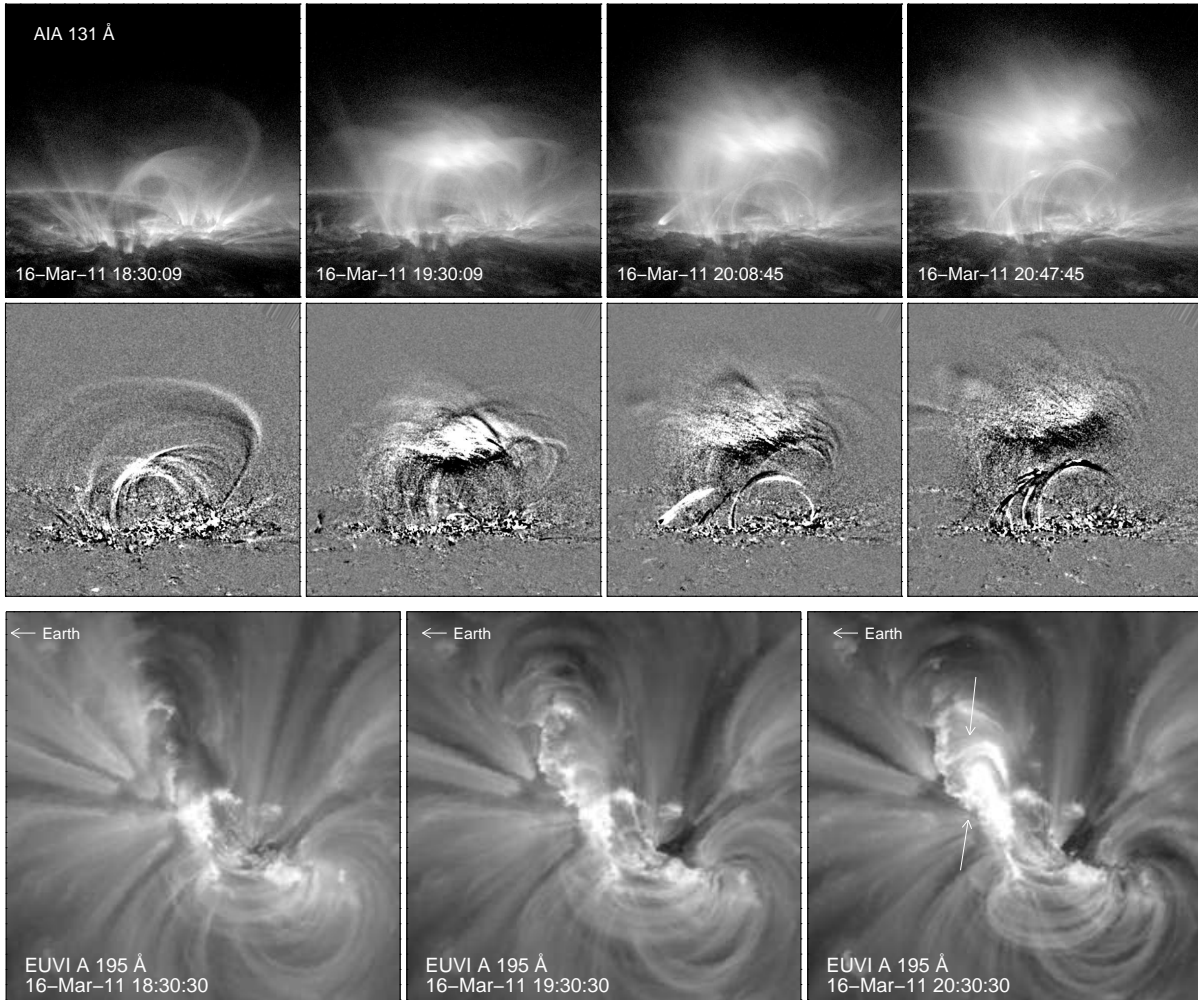
FIG. 2.— Observations of a limb flare with AIA and EUVI on 2011 March 16. The top panels show the AIA 131 Å intensities scaled logarithmically at various times during the event. The middle panels show the running difference images for these times. The field of view of the AIA images is $350'' \times 319''$ and the image has been rotated. Details on how the running difference images are computed are given in the text. The bottom panels show the EUVI images from the A spacecraft. The size of the EUVI field of view is $408'' \times 408''$. The arrows in the final panel of the EUVI images indicates the approximate orientation of the flare ribbons. The electronic version of the manuscript contains a movie of the running difference images.

downflows much more clearly than the raw intensity images. In general, the downflows appear as dark features in the running difference images, indicating that they are dark relative to the emission into which they are descending.

2.1. *Morphology of the Downflows*

In the March 16 event all of the downflows appear as elongated loop-like features. As illustrated in the example shown in Figure 5, when the loops first appear they are relatively broad but they are compressed as they descend. Many of the descending loops that are the easiest to observe appear relatively late in the event (after approximately 20:00 UT). At earlier times, 18:20–19:00 UT for example, high temperature emission appears at relatively low heights very suddenly and does not appear to descend from larger heights. The loops that appear near 18:30 UT and are shown in the first column of Figure 2 illustrate this. There is, however, some downward motion after the emission appears, consistent with the shrinkage of post-reconnection loops (e.g., Forbes & Acton 1996).

Some of the downflows in these events are observed as dark voids during the entirety of their descent. This is true for almost all of the downflows observed in the May 9 event. As

with the loops observed in the March 16 event, the voids are relatively wide when they appear and are compressed in size as they descend. An example downflow is shown in Figure 5. The timing of the downflows is similar to that of the March 16 event, with many of the most easily observed downflows being observed somewhat later in the evolution of the flare. Many downflows are observed after 21:15 UT, which is after the peak of the *GOES* soft X-ray flux.

In the May 18 event a mixture of descending voids and loops is observed. For this flare there are also some downflows that evolve from voids into loops. An example of a downflow that begins as a void and evolves into a loop is shown in Figure 5. The earliest high temperature emission in this event is also observed to appear very suddenly at low heights without any downward motion as the loops brighten. After these loops appear, they do to contract downward to lower heights. As in the March 16 flare, most of the downflows that are easily observed appear after the peak of the soft X-ray emission.

The *STEREO* observations suggest that the orientation of the May 18 event is particularly interesting. The third panel of Figure 4 shows that the post-flare loop arcade forms an "Γ"
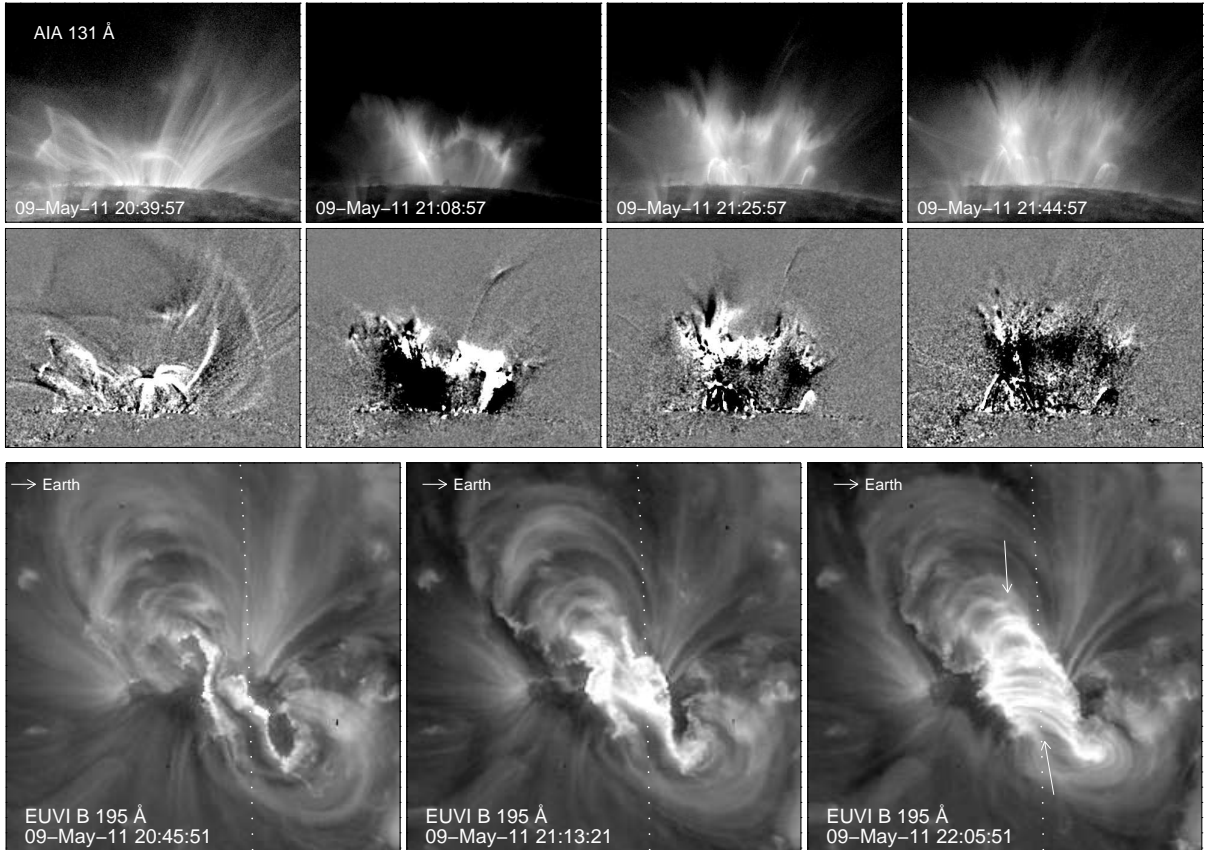
FIG. 3.— The same as in Figure 2, but for the 2011 May 9 event. The field of view of the AIA images is $301'' \times 229''$ and the image has been rotated. The EUVI data are from the B spacecraft. The dotted line indicates the position of the limb as viewed from Earth. The size of the EUVI field of view is $409'' \times 409''$. The electronic version of the manuscript contains a movie of the running difference images.

shape, with part of the "Γ" oriented parallel to the line of sight and another part oriented perpendicular to it. When the axis of the arcade is along the line of sight the downflows appear as loops or as voids that transition to loops. *STEREO* observations indicate that the other events are consistent with this interpretation. The arcade in the March 16 event is oriented at an angle to the line of sight and loops are observed (see Figure 2). The arcade in the May 9 event is essentially perpendicular to the line of sight and only voids are observed (see Figure 3).

For each event we also inspected the 94 Å images. As noted earlier, this channel includes a strong Fe XVIII emission line and is sensitive to somewhat lower temperature plasma than the 131 Å channel. As one would expect, these images tend to show the somewhat cooler plasma at the lower part of the arcade and as a result tend to show the terminal phase of the downflows. For this reason we focus on the data from the AIA 131 Å channel in this paper.

2.2. *Height-Time Maps*

A useful way of tracking features as they descend is to create height-time maps. These maps are formed by extracting a narrow "slit" from each image and stacking them horizontally as a function of time (see Sheeley et al. 2004). Interpolation is used to extract intensities at arbitrary angles. An example height-time map computed from the difference images is shown in Figure 6. Here the downflows are evident as dark tracks, indicating that the downflows are generally less intense than the emission into which they are descending.

To characterize the kinematics of the downflows we fit selected height-time tracks to a function of the form

$$h(t) = h_0 + v_T t + a_0 \tau^2 (e^{-t/\tau} - 1). \tag{1}$$

With this assumption the velocity of the downflow as a function of time is

$$v(t) = v_T - a_0 \tau e^{-t/\tau}, \tag{2}$$

and the acceleration is

$$a(t) = a_0 e^{-t/\tau}. \tag{3}$$

This functional form for the height captures the rapid transition from a relatively high initial velocity of $v(t = 0) \approx -a_0\tau$ at a height of h_0, to a relatively slow terminal descent, v_T. Note that for features that descend at progressively slower speeds the initial velocity will be negative and the acceleration will be positive.

We have selected approximately 10 downflows from each event and traced out their tracks in the height-time maps. The best-fit parameters for Equation 1 were determined for each track using a least-squares algorithm and are given in Table 1. Each track is also indicated in the movies included in the electronic version of the manuscript.

We tended to select high velocity tracks that appeared at relatively large heights since they were easier to track and are more relevant to the initial dynamics of post-reconnection flux tubes. Many of the tracks that we selected decelerate quickly and could not be followed for long periods of time.
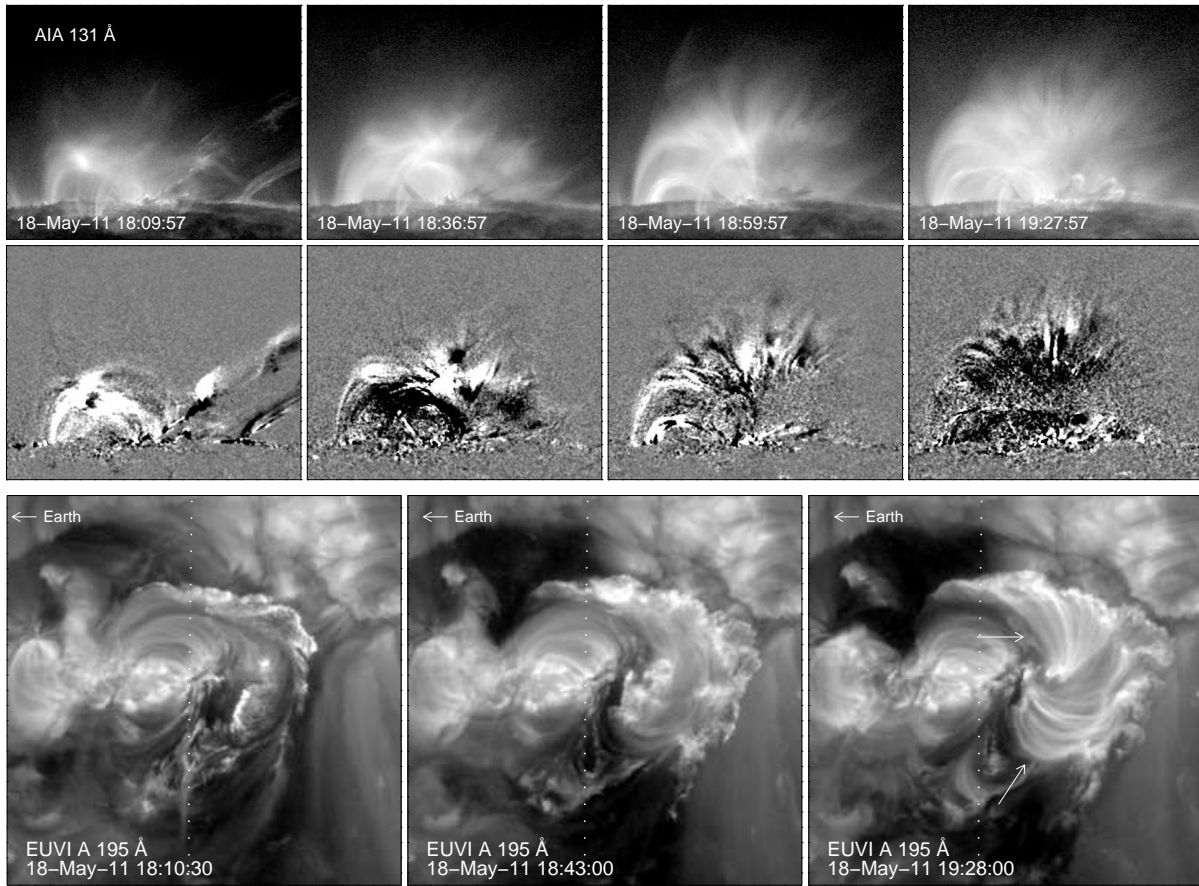
FIG. 4.— The same as in Figure 2, but for the 2011 May 18 event. The field of view of the AIA images is $277'' \times 187''$ and the image has been rotated. The EUVI data are from the A spacecraft. The dotted line indicates the position of the limb as viewed from Earth. The size of the EUVI field of view is $408'' \times 408''$. The electronic version of the manuscript contains a movie of the running difference images.
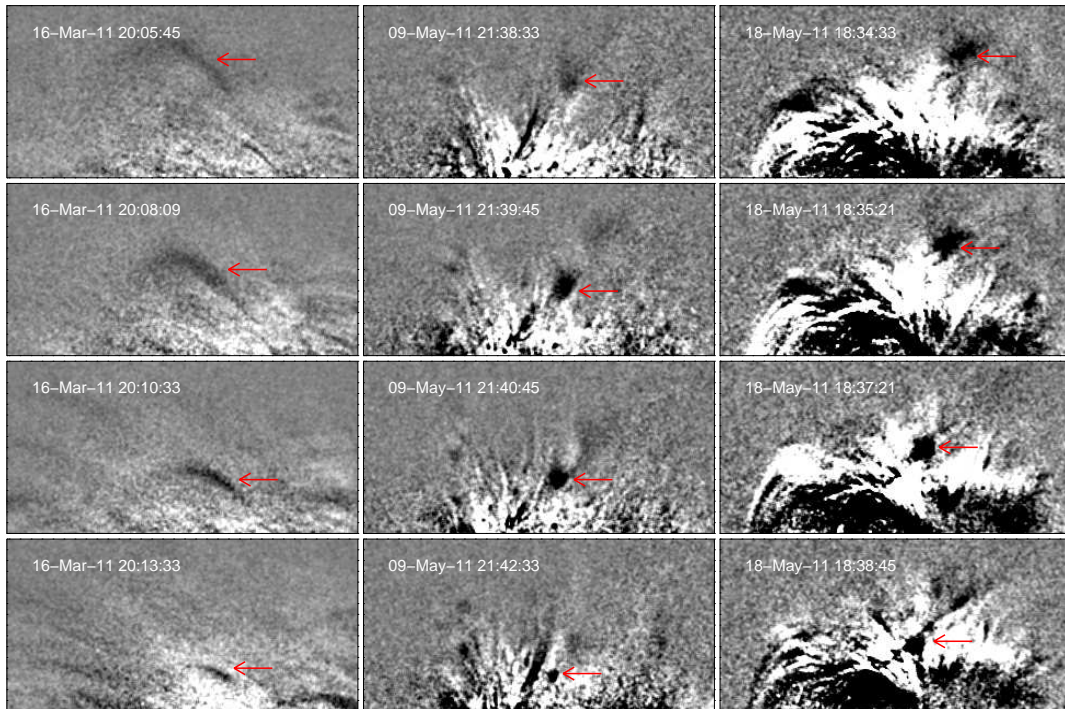

FIG. 5.— Example inflows observed with AIA. The left panels shows a descending loop-like feature from the March 16 event. The middle panels shows a descending void from the May 9 flare. The right panels are from the May 18 event.
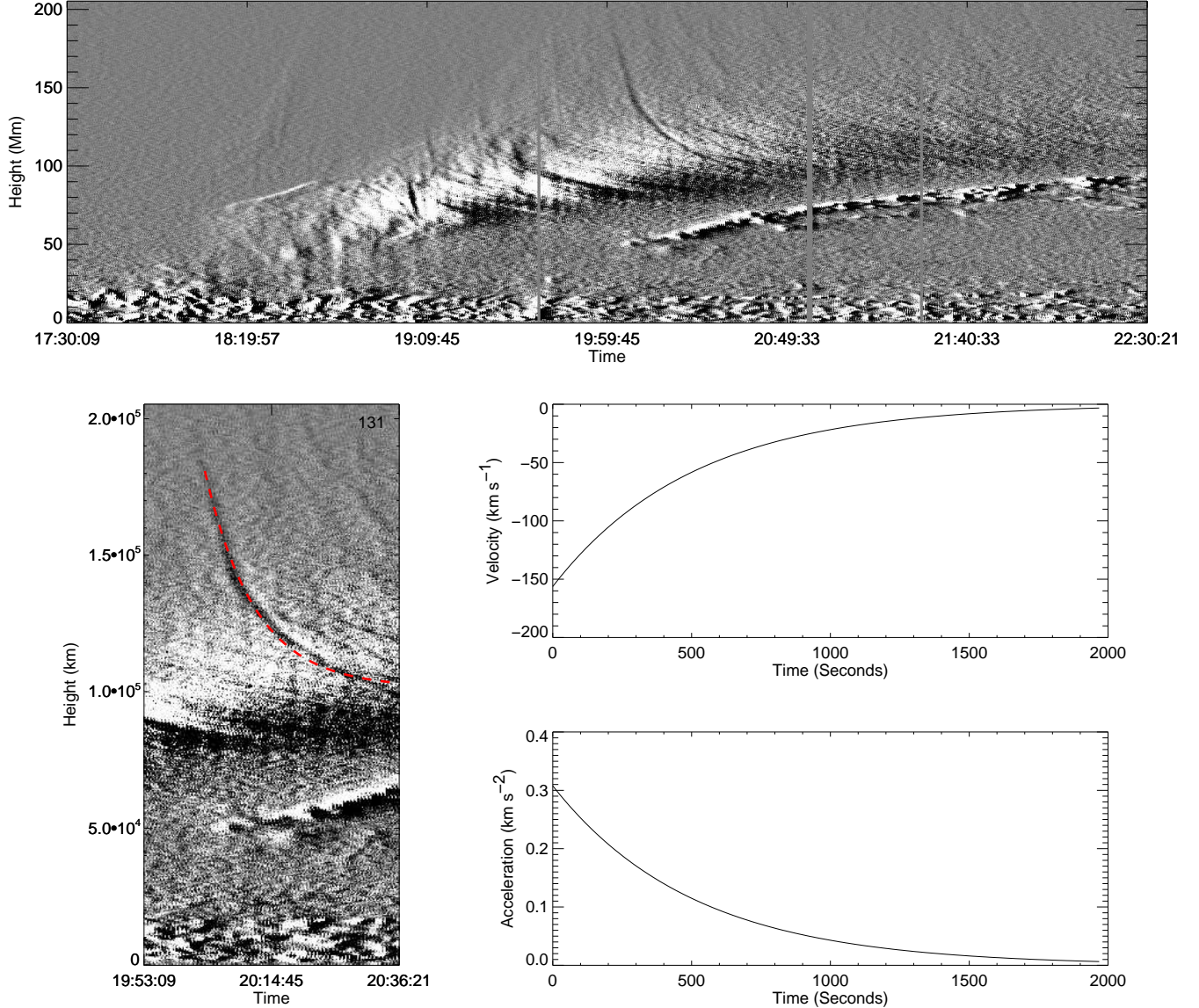
FIG. 6.— An example AIA 131 Å height-time map. The top panel shows the height-time map for most of the event. This figure illustrates some basic features common to all of the events: The rapid expansion of the hot plasma (about $40\,\mathrm{km\,s^{-1}}$), the dark tracks of the inflows that descend into the hot plasma, and the formation of cool, post-flare loops at the bottom of the arcade. The rise of the cool post-flare loops is initially rapid ($10\,\mathrm{km\,s^{-1}}$), but gradually decelerates to about $2\,\mathrm{km\,s^{-1}}$ toward the end of the observations. The bottom panels show an expanded view of the downflow of interest and the kinematic information derived from the height-time track. This is track number 7 from 2011 March 16 (see Table 1).

This means the asymptotic behavior is not well observed for these tracks. If we leave v_T as a free parameter in the fitting of these tracks the terminal velocity often converges to relatively large number, inconsistent with the general trend in the data. For tracks that do have a well observed terminal phase, the terminal velocity is typically about 4–$5\,\mathrm{km\,s^{-1}}$. Since the terminal velocities are generally small and we are more interested in the initial dynamics we have forced $v_T = 0$ for the final fits given in Table 1.

With the improved imaging capabilities of AIA we anticipated being able to track downflows at larger heights above the solar surface. Comparing the values for h_0 given in Table 1 with Figures 6 from Savage & McKenzie (2011) we see that is the case. Our median initial height is approximately 111 Mm compared with 82 Mm with the earlier data.

Our initial velocities and accelerations, however, are very similar to those presented by Savage & McKenzie (2011) in their Figure 5. For the initial velocity we have a median value of $-144\,\mathrm{km\,s^{-1}}$ compared with $-146\,\mathrm{km\,s^{-1}}$ in Savage & McKenzie (2011). Our median initial acceleration is $0.68\,\mathrm{km\,s^{-2}}$ compared with $0.42\,\mathrm{km\,s^{-2}}$. Thus it appears that small initial velocities relative to the Alfvén speed are not an artifact of the lower heights at which the downflows have been observed previously.

Chromospheric evaporation is an essential component of solar flares models based on magnetic reconnection (e.g., Fisher et al. 1985). The release of energy on reconnected field lines will ultimately lead to the heating and evaporation of chromospheric material. This should lead to loops that brighten over time and numerical simulations suggest that this

TABLE 1
INFLOW PROPERTIES

Track	h_0 (Mm)	a_0 (km s^{-2})	τ (s)	v_0 (km s^{-1})
16 March 2011				
00	132.6	0.039	831.7	-32.1
01	149.0	2.282	119.0	-271.6
02	178.6	0.274	454.1	-124.5
03	196.6	0.492	290.6	-143.0
04	204.3	0.857	226.7	-194.2
05	136.5	0.619	261.2	-161.7
06	188.9	0.271	500.6	-135.8
07	180.9	0.308	507.7	-156.2
08	225.6	0.089	1031.3	-91.7
09	250.4	0.044	1938.6	-84.6
9 May 2011				
00	113.6	2.185	128.1	-279.9
01	118.9	1.043	212.5	-221.7
02	131.1	1.506	166.6	-250.9
03	117.6	0.581	231.3	-134.3
04	128.2	0.440	345.3	-152.1
05	110.8	0.161	406.1	-65.3
06	63.8	0.087	659.1	-57.1
07	82.0	0.237	363.8	-86.1
08	80.4	1.050	115.6	-121.3
09	103.7	0.786	192.2	-151.1
10	73.8	0.306	245.1	-75.1
11	90.9	0.375	270.7	-101.7
18 May 2011				
00	75.2	2.687	102.1	-274.4
01	84.7	2.726	97.1	-264.8
02	83.3	0.451	274.1	-123.7
03	70.5	3.407	77.7	-264.8
04	61.7	1.190	120.0	-142.8
05	75.1	0.867	165.8	-143.7
06	88.3	0.473	316.6	-149.9
07	70.7	1.059	155.9	-165.0
08	76.7	0.438	243.4	-106.5
09	83.1	0.403	440.2	-177.0

process should occur rapidly (e.g., Mariska et al. 1989). One limitation of the running difference images is that they can obscure the evolution of the absolute intensities. The downflows are dark features in the running difference images, indicating that they have lower intensities than the surrounding emission. It is not clear, however, if they remain dark in an absolute sense or brighten over time.

To address this issue we have followed the intensities along each track in the unsubtracted images. For comparison we also determined intensities at several locations outside of the track. In all cases the intensity in the center of the feature simply tracks the background intensities measured outside of the downflow. There is no evidence for the intensities in the downflows rising faster than the background. Unfortunately, these measurements are difficult to make and subject to considerable uncertainty. The downflows have a very low contrast relative to the ambient emission in the flare. The difference images shown in Figures 2–6 are all scaled over a range of about ± 5 DN s^{-1}, which is typically only a few percent of the absolute intensity.

3. DISCUSSION

We have presented the first observations of supra-arcade downflows with the AIA instrument on *SDO*. With the new capabilities of AIA we are able to track inflows at much larger heights and for much smaller events than in previous observations. These observations provide many new examples of features forming at large heights and descending onto the accumulating post-flare loop arcade. The dynamics and morphology of the downflows provides compelling evidence for the role of magnetic reconnection in eruptive solar flares.

Despite the qualitative agreement between the observations and the standard picture of magnetic reconnection, there are several problems that remain. The low velocities that are observed for these outflows, for example, are incompatible with the simple 2D models of Sweet-Parker and Petschek reconnection, which have Alfvénic velocities for the outflows. Linton & Longcope (2006) suggest that the interaction of the reconnected flux tubes with pre-existing magnetic fields provide a drag force that slows the downflows.

Another difficulty in interpreting the downflows as evidence for magnetic reconnection is the formation of the initial flare plasma. For most events the downflows that are easily observed occur late in the flare and descend into an existing cloud of hot emission. The initial flare emission forms essentially "in place," and not as a descending loop — although there is some evidence for collapsing motions after these loops appear.

Finally, the reconnection of magnetic fields should lead to the release of energy that drives chromospheric evaporation. All of the downflows that we detect here, however, are observed as depletions relative to the ambient high temperature emission into which they are descending. Recent work by Guidoni & Longcope (2011) suggests that density depletions can be formed in reconnecting flux tubes that move through a nonuniform current sheet. Their model, however, does not include chromospheric evaporation and it is not clear how long such density depletions would persist.

The inability of the simple, two-dimensional reconnection models to describe many details of the downflows suggests that three-dimensional modeling is required. The AIA observations we have shown here give ample evidence for inhomogeneity in the reconnecting magnetic fields and this inhomogeneity will be a component of any successful model. High resolution observations of the photospheric magnetic field in active regions, such as those taken with the Solar Optical Telescope (SOT) on *Hinode* (e.g, Kubo et al. 2007), show that the magnetic field is structured on the spatial scale of the granules (~ 1000 km) and we conjecture that this inhomogeneity is reflected in the highly structured appearance of the flare plasma.

REFERENCES

Asai, A., Yokoyama, T., Shimojo, M., & Shibata, K. 2004, ApJ, 605, L77
Fisher, G. H., Canfield, R. C., & McClymont, A. N. 1985, ApJ, 289, 414
Forbes, T. G., & Acton, L. W. 1996, ApJ, 459, 330
Guidoni, S. E., & Longcope, D. W. 2011, ApJ, 730, 90
Howard, R. A., et al. 2008, Space Sci. Rev., 136, 67
Innes, D. E., McKenzie, D. E., & Wang, T. 2003, Sol. Phys., 217, 247
Kubo, M., et al. 2007, PASJ, 59, 779
Lemen, J. R., et al. 2011, Sol. Phys., 115

Linton, M. G., & Longcope, D. W. 2006, ApJ, 642, 1177
Mariska, J. T., Emslie, A. G., & Li, P. 1989, ApJ, 341, 1067
McKenzie, D. E., & Hudson, H. S. 1999, ApJ, 519, L93
O'Dwyer, B., Del Zanna, G., Mason, H. E., Weber, M. A., & Tripathi, D. 2010, A&A, 521, A21
Savage, S. L., & McKenzie, D. E. 2011, ApJ, 730, 98
Savage, S. L., McKenzie, D. E., Reeves, K. K., Forbes, T. G., & Longcope, D. W. 2010, ApJ, 722, 329

Sheeley, N. R., Jr., Knudson, T. N., & Wang, Y.-M. 2001, ApJ, 546, L131
Sheeley, N. R., Jr., & Wang, Y.-M. 2001, ApJ, 562, L107
Sheeley, N. R., Jr., Warren, H. P., & Wang, Y.-M. 2004, ApJ, 616, 1224
Wang, Y.-M., Sheeley, N. R., Howard, R. A., St. Cyr, O. C., & Simnett,
  G. M. 1999, Geophys. Res. Lett., 26, 1203

Warren, H. P., Bookbinder, J. A., Forbes, T. G., Golub, L., Hudson, H. S.,
  Reeves, K., & Warshall, A. 1999, ApJ, 527, L121
Zweibel, E. G., & Yamada, M. 2009, ARA&A, 47, 291